Journal of Alloys and Compounds 502 (2010) 118–122

Contents lists available at ScienceDirect

Journal of Alloys and Compounds

journal homepage: www.elsevier.com/locate/jallcom

Large-scale preparation of chestnut-like ZnO and Zn–ZnO hollow nanostructures by chemical vapor deposition

S.L. Wang*, X. Jia, P. Jiang, H. Fang, W.H. Tang

Department of Physics, Center for Optoelectronics Materials and Devices, Zhejiang Sci-Tech University, Hangzhou 310018, PR China

ARTICLE INFO

Article history:
Received 17 November 2009
Received in revised form 7 April 2010
Accepted 7 April 2010
Available online 14 April 2010

Keywords:
ZnO
Zn–ZnO
Chestnut-like
Growth mechanism
Photoluminescence

ABSTRACT

Large-scale chestnut-like ZnO and Zn–ZnO hollow nanostructures on Si substrates were prepared without catalyst by a one-step chemical vapor deposition technique. The morphology, composition, and phase structure of as-prepared products were characterized by scanning electron microscopy, energy-dispersive X-ray spectrometry, and X-ray diffraction, respectively. The ZnO consists of chestnut-like nanostructures with hollow interior and a lot of nanoneedles aligning on the surface of the hollow structure in a radial way, whereas the Zn–ZnO shows that long nanowires grew on the chestnut-like hollow structure with a hexagonal flower-like structure on the top layer. A vapor–solid (VS) growth mechanism for the chestnut-like ZnO and Zn–ZnO hollow nanostructures was proposed. The photoluminescence (PL) of ZnO and Zn–ZnO shows a large number of oxygen vacancy defects appeared in the novel hollow nanostructures.

1. Introduction

Zinc oxide (ZnO) is a wide direct band gap (3.37 eV) semiconductor with large exciton binding energy (60 meV) at room temperature, which has a great potential application in optoelectronic filed [1], such as photocatalyst [2], sensors [3], light-emitting diodes [4–6], solar cells [7,8], and so on. It is well-known that many physical properties of nanostructures are strongly dependent on morphologies [9]. Thus, various kinds of ZnO nanostructures were developed to improve their physical properties, such as nanowires [10], nanorings [11], nanorods [12], nanobelts [13], nanosheets [14] and nanodiscs [15]. Especially, ZnO hollow nanostructures represent useful applications in many fields due to their low density, large specific surface area, and interesting optical properties [16,17]. Many strategies have been developed for preparing hollow structures, such as templates [18,19], vapor–solid (VS) [20], and liquid–solid (LS) growth mechanism [21]. Deng et al. [22] fabricated ZnO hollow spheres by a facile solution method using sulfonated polystyrene core–shell spheres as the template, and the core could be easily removed without additional dissolution or calcination process. Sulieman et al. [23] reported the growth and structural properties of hollow-opened ZnO/Zn and solid Zn/ZnO single crystal microspheres on a silicon (1 1 1) substrate by chemical vapor deposition. Later, Liu et al. [24] prepared porous ZnO hollow structures with tunable diameters and shell thicknesses by thermal evaporation. Although much progress has been made in the synthesis of hollow structures, it still remains a challenge to develop a facile, catalyst-free, one-step route for fabricating large-scale inorganic hollow nanostructures.

The vapor–liquid–solid (VLS) mechanism has been widely applied to the growth of ZnO nanostructures [25,26]. However, it needs high growth temperatures (about 1000–1200 °C) and catalysts [10,27], which have limited its application greatly. In this work, diverse morphologies, such as chestnut-like, flower-like and hexagonal polyhedron ZnO and Zn–ZnO hollow nanostructures on Si substrates were prepared without using any catalyst by a simple chemical vapor deposition (CVD) at a lower temperature. The possible growth mechanisms for chestnut-like ZnO and Zn–ZnO hollow nanostructures were proposed.

2. Experimental

N-type Si (0 0 1) substrates (1.5 cm × 1.5 cm) were ultrasonically cleaned in hydrochloric acid solution, acetone and deionized water for 30 min, respectively. Commercial Zn powder (1.0 g) with a purity of 99.999% was used as the source material and put in an alumina boat (Boat A), whereas several pieces of Si substrates were placed in another alumina boat (Boat B). These two boats were loaded into a furnace with a horizontal alumina tube (as shown in Fig. 1a). Two ends of the tube were sealed using mechanically clamped steel plates with the rubber gaskets. The tube was evacuated by a mechanical rotary pump, purged with 500 sccm of argon. Then the furnace temperature was raised to 1000 °C at a rate of ~20 °C/min with introducing oxygen gas into the chamber. After reaction for 1 h, the furnace was cooled down to room temperature naturally. Detailed reaction parameters for other products were shown in Table 1. The substrate temperature was measured by thermocouple in different position in the tube (Fig. 1b).

The crystallographic information of the prepared samples was analyzed by powder X-ray diffraction (XRD) using a Bruker AXS D8 DISCOVER X-ray diffrac-

* Corresponding author. Tel.: +86 571 86843574; fax: +86 571 86843248.
E-mail address: slwang@zstu.edu.cn (S.L. Wang).

0925-8388/$ – see front matter © 2010 Elsevier B.V. All rights reserved.
doi:10.1016/j.jallcom.2010.04.042

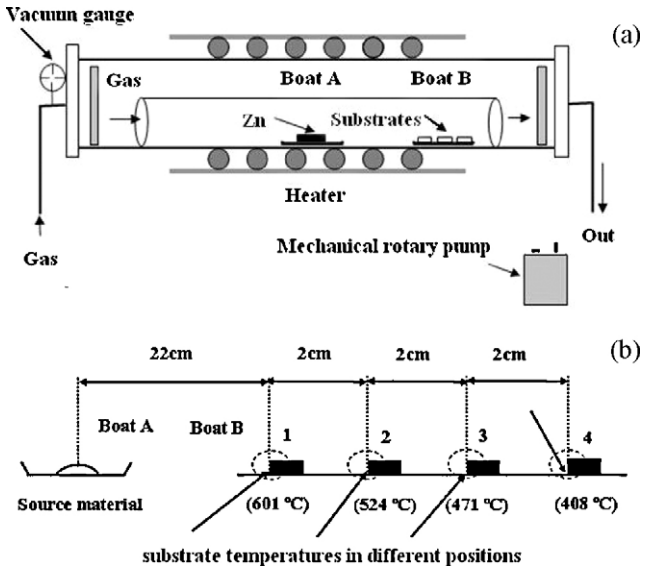

Fig. 1. (a) Schematic diagram of the horizontal furnace and (b) substrate temperatures in different positions.

tometer with Cu Kα radiation (λ = 1.5406 Å). The morphology and composition of the as-deposited products were characterized by field emission scanning electron microscope (FESEM, S-4700) and energy-dispersive X-ray spectrometry (EDX),

Table 1
Samples obtained at different conditions.

Sample	Substrate temperature (°C)	O_2 (sccm) (before cooling process/in cooling process)
S1	601	70/70
S2	524	70/70
S3	471	50/50
S4	408	50/50
S5	524	70/0

respectively. Photoluminescence properties of chestnut-like ZnO and Zn–ZnO hollow nanostructures were measured on a FLSP920 fluorescence spectrometer using a Xe lamp with the excitation wavelength of 320 nm at room temperature.

3. Results and discussion

Fig. 2 shows FESEM images of the products prepared under different conditions. As shown in Fig. 2a, a deformed chestnut-like hollow microstructure was obtained at 601 °C (S1), which consists of a hollow cavity interior and some short nanoneedles on the outside surface. Fig. 2b and c shows FESEM images of the product (S2) obtained at 524 °C. The chestnut-like structures with nanoneedles on their surface were shown in Fig. 2b. Fig. 2c shows the high magnification FESEM image of a perfect individual chestnut-like structure, which was composed of a sphere-like hollow structure (5–6 μm in diameter), and a lot of nanoneedles (20–40 nm in tip, 80–150 nm in root and 1–5 μm in length) aligning on the surface

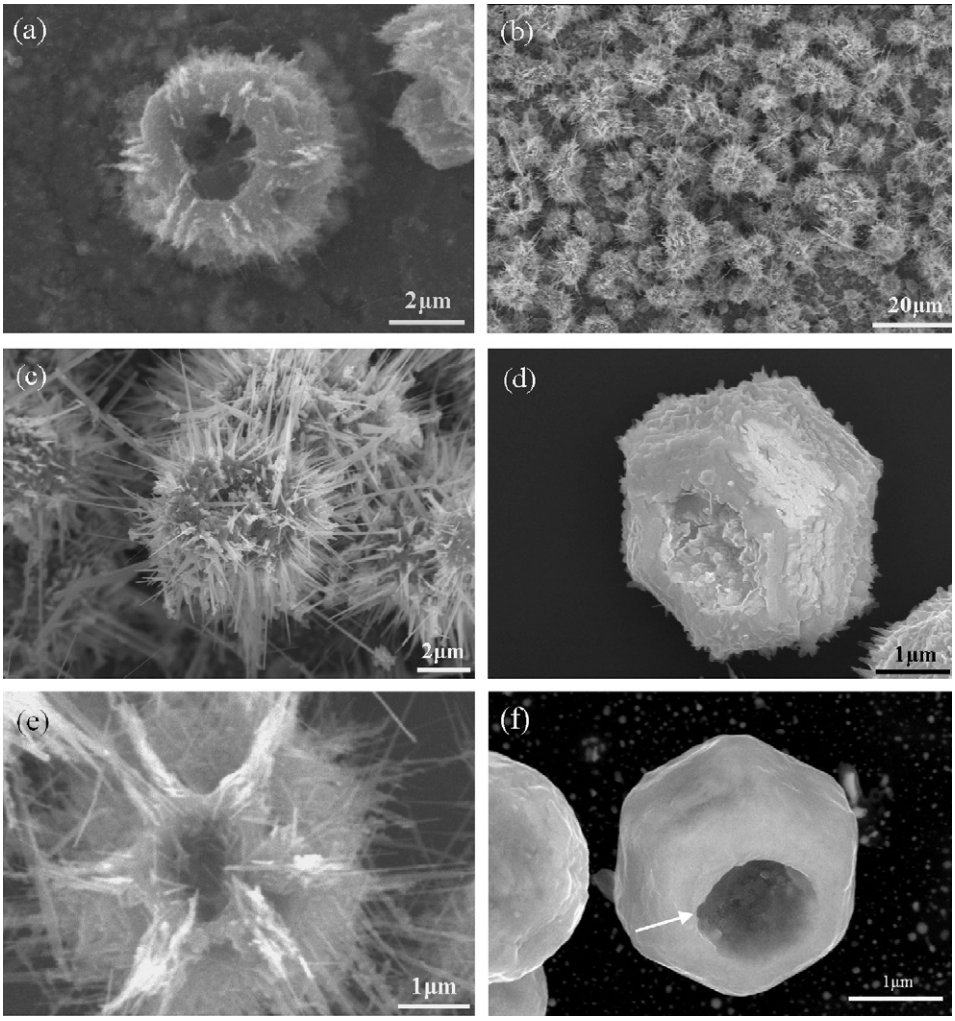

Fig. 2. FESEM images of samples obtained at different temperatures: (a) 601 °C, (b and c) 524 °C, (d) 471 °C, (e) 408 °C, and (f) 524 °C, no oxygen in the cooling process.

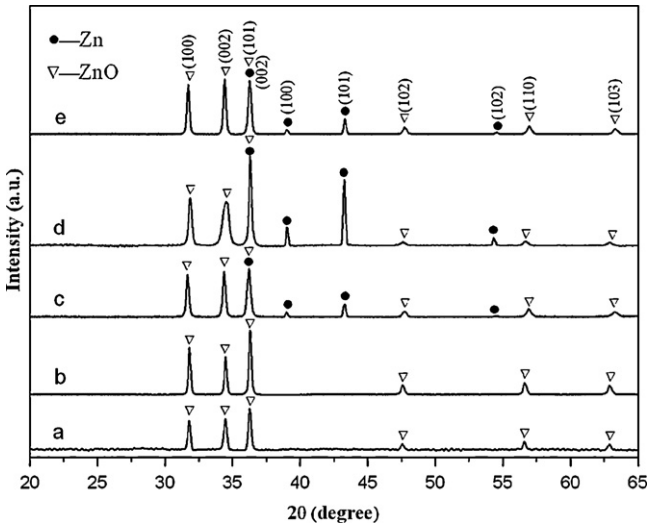

Fig. 3. XRD patterns of the as-prepared samples (a–f) for S1–S5, respectively.

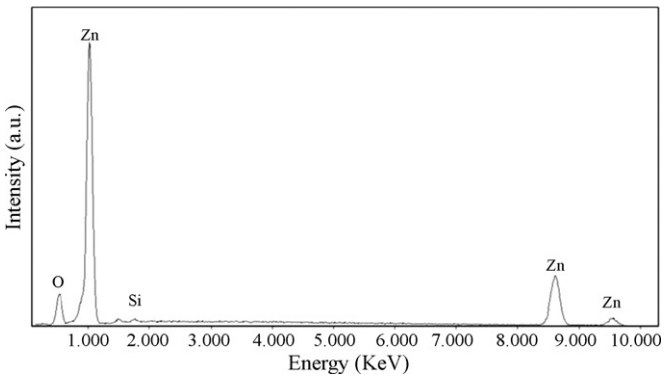

Fig. 4. EDX spectrum of S2 obtained at 524 °C.

of the hollow structure in a radial way. Fig. 2d and e displays the products obtained at lower temperature regions, about 471 °C and 408 °C, respectively. As shown in Fig. 2d, the product (S3) consists of a series of hexagonal layers with a hexagonal cavity interior and some short nanoneedles on the outside surface. The product (S4) obtained at 408 °C shows that long nanowires grew on the chestnut-like hollow structure with a hexagonal flower-like structure on the top layer (Fig. 2e). Fig. 2f shows the FESEM image of the product (S5) obtained at 524 °C without oxygen in the cooling process. The morphology of the product was a hexagonal polyhedron with a sphere-like hollow structure interior and without any nanoneedles on the surface.

XRD and EDX analysis were utilized to analyze the crystal structure and elemental composition of the resulting samples, respectively. Fig. 3 shows the XRD patterns of the products under different synthetic conditions. Fig. 3a and b shows the XRD patterns of S1 (601 °C) and S2 (524 °C), respectively. All the diffraction peaks can be indexed to wurtzite hexagonal ZnO (JCPDS Card file no. 70-2551). Fig. 3c–e shows the XRD pattern of S3 (471 °C), S4 (408 °C) and S5 (524 °C, without oxygen in the cooling process), respectively. Hexagonal Zn (JCPDS Card file no. 65-3358), and ZnO (JCPDS Card file no. 70-2551) peaks were detected. The EDX spectrum of S2 was represented in Fig. 4, in which the chestnut-like hollow nanostructures are composed only of Zn and O, and this result is in good accordance with the XRD analysis. The appearance of Si peak in the spectrum is due to the substrate.

Base on the experimental results (SEM, XRD and EDX) mentioned above, the possible growth mechanisms of the chestnut-like ZnO and Zn–ZnO hollow nanostructures were proposed (as shown in Fig. 5). It may consist of three stages: (1) formation of the Zn polyhedrons; (2) surface oxidation; and (3) formation of the hollow structure and growth of the ZnO nanostructures (nanoneedles and nanowires) on ZnO layers.

Two types of Zn polyhedrons were obtained on Si (1 1 1) substrates in the experiments (Fig. 2d and f), which were similar to Chen's work [28]. The formation of Zn polyhedron includes nucleation and growth of Zn on Si substrate. First, the vaporized Zn powder transported downstream and deposited on the Si substrates. Then, these Zn atoms were aggregated to form the Zn droplets and nucleated on the surface of Si substrate. Thus, the Zn nuclei grew in the direction of arrow (as shown in Fig. 5). The minimum free energy, consisting of surface, interfacial, and strain energy is a crucial role on the growth of Zn polyhedrons with different types [29,30]. Therefore, the lower total free energy maybe the higher probability of forming a certain type Zn polyhedrons.

In addition, according to the growth kinetics, rearrangement of the sublattices of zinc from hexagonal Zn to hexagonal ZnO will occur on the surface of Zn nanocrystals following the Zn template [31]. When the oxygen was introduced, the ZnO layers were quickly formed on the surface of Zn polyhedrons by surface oxidation and steadily grew in the direction of arrow (Fig. 5).

While the annealing temperature is higher than 500 °C, the ZnO layers of core–shell Zn–ZnO polyhedrons can be deformed and collapsed because the melting point of Zn is about 410 °C [28,32]. Based on the results in the experiments, schematic diagrams for the formation of different hollow structures were presented (Fig. 6). When the substrate temperature increased from 408 °C to 471 °C, the ZnO layer of core–shell Zn–ZnO polyhedrons was expanded slightly, which caused slight deformation of the Zn–ZnO micron structures, and the deformation may be ascribed to the strain induced by phase transformation in oxidation process [33]. In the cooling process, there is a crack at the interface of Si and Zn–ZnO polyhedron, due to the different thermal expansion coefficient [28], which provides convenience for the re-evaporation of Zn. As a result, the top of ZnO layers was broken and the partial hollow structures were formed (Fig. 2d and e). When the substrate temperature was further

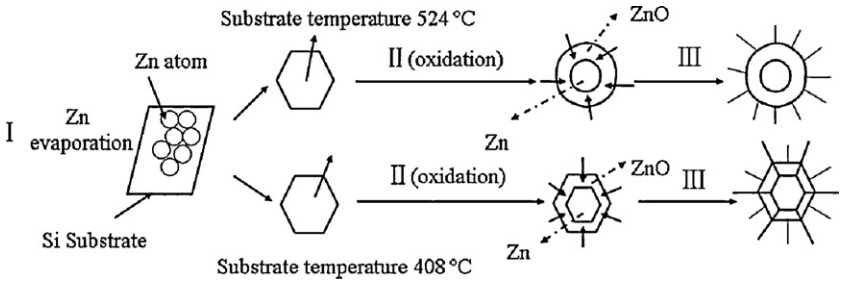

Fig. 5. Growth mechanism diagram of the as-prepared products.

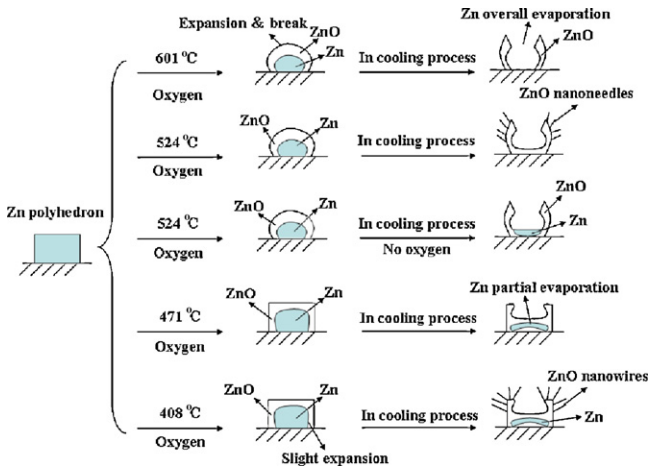

Fig. 6. The schematic diagrams for the formation of different hollow structures.

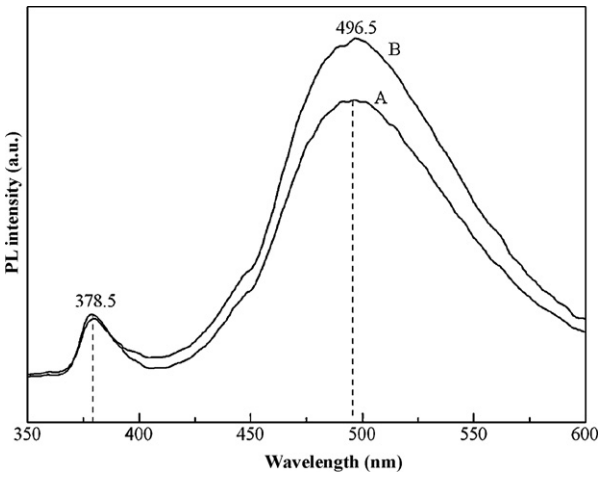

Fig. 7. Photoluminescence spectra of the synthesized products (A) chestnut-like ZnO hollow nanostructures (S2) and (B) flower-like Zn–ZnO hollow nanostructures (S4).

increased to 524 °C, the phase transformation-induced strain (i.e., volume expansion) [33] caused the top of Zn–ZnO micron structures to break in cooling process. Subsequently, the Zn core was re-evaporated through the cracks in the top faces (Fig. 2c). With the increasing of substrate temperature, more Zn was re-evaporated, and the crack became larger (Fig. 2a), as well as the cracks at the interface of Si and Zn–ZnO polyhedron, which promoted the re-evaporation of Zn core [28]. Thus, the hollow polyhedrons were formed by the re-evaporation of Zn core.

During the cooling process, the ZnO nanostructures such as nanoneedles or nanowires grew on the ZnO surface with the sustained oxygen gas according to following reactive equations:

$$Zn_{(s)} \rightarrow Zn_{(g)} \quad (1)$$

$$2Zn_{(g)} + O_2 \rightarrow 2ZnO_{(s)} \quad (2)$$

As shown in the two reactive equations, the oxygen gas is a crucial factor on the formation of ZnO nanostructures. Only the hollow polyhedron without any nanoneedle or nanowire could be obtained (Fig. 2f), when no oxygen was introduced. The substrate temperature is another important factor on the growth of ZnO nanoneedles and nanowires. Under the same oxygen carrier gas flow, the lower substrate temperature (about 524 °C and 408 °C, respectively) promoted the growth of ZnO nanoneedles and nanowires in length (compared with Fig. 2a and c–e). This is possibly due to the high deposition ratio of oxygen atoms in lower temperature region. Considering that no catalyst was used, the possible growth mechanism of ZnO nanoneedles and nanowires is a vapor–solid mechanism [34]. When the oxygen was introduced, the ZnO nuclei were initially formed on the surface of Zn droplets and these ZnO nuclei grew in the direction of the ZnO layers in form of ZnO nanoneedles and nanowires subsequently.

Fig. 7 shows the room temperature PL spectra recorded from samples S2 and S4. As shown in pattern A, the sharp peak at 378.5 nm corresponds to the near-band-edge emission of ZnO, which is attributed to the recombination of free excitations [35]. Whereas, the peak at 496.5 nm corresponding to the deep-level emission is associated with defects in ZnO lattice, such as oxygen vacancy and Zn interstitials [31,35]. Therefore, the deep-level emission (pattern A, S2, ZnO) may indicate the existence of oxygen vacancies in the hollow structure and the nanostructures. To compare with the pure ZnO, the relatively large lattice mismatch between Zn and ZnO (17%) could be induced, which became the defect generator and caused the strong deep-level emissions in the interface [31]. Thus, the stronger deep-level emission at 496.5 nm observed in pattern B (S4, Zn–ZnO) may be ascribed to the oxygen vacancy and Zn interstitials together. This significant defect-related emission property of ZnO nanostructures may be beneficial to their photocatalytic activity.

4. Conclusions

Large-scale chestnut-like hollow ZnO and Zn–ZnO nanostructures on Si substrates were prepared without catalyst by a one-step CVD technique. Various morphologies were obtained by adjusting the concentration of oxygen gas and the substrate temperature. The possible growth mechanism was proposed and it may consist of three stages: (1) formation of the Zn polyhedrons, (2) surface oxidation, and (3) formation of the hollow structure and growth of ZnO nanostructures on ZnO layers. The photoluminescence spectrums indicate a large number of oxygen vacancy and/or Zn interstitials defects in the chestnut-like ZnO and Zn–ZnO hollow nanostructures.

Acknowledgements

This work was supported by the National Basic Research Program of China (973 Program) (Grant No. 2010CB933501), the Innovative Youth Team of Natural Science Foundation of Zhejiang Province (Grant No. R4090058) and the Ministry of Education of Zhejiang Province (Grant No. Y200806012).

References

[1] M.K. Lee, H.F. Tu, Optical emissions of Zn and ZnO in Zn–ZnO structure synthesized by electrodeposition with aqueous solution of zinc nitrate-6-hydrate, Cryst. Growth Des. 8 (2008) 1785–1788.
[2] T.J. Kuo, C.N. Lin, C.L. Kuo, M.H. Huang, Growth of ultralong ZnO nanowires on silicon substrates by vapor transport and their use as recyclable photocatalysts, Chem. Mater. 19 (2007) 5143–5147.
[3] X.D. Wang, J. Zhou, J.H. Song, J. Liu, N.S. Xu, Z.L. Wang, Piezoelectric field effect transistor and nanoforce sensor based on a single ZnO nanowire, Nano Lett. 6 (2006) 2768–2772.
[4] K. Keem, D.Y. Jeong, S. Kim, M.S. Lee, I.S. Yeo, U.I. Chung, J.T. Moon, Fabrication and device characterization of omega-shaped-gate ZnO nanowire field-effect transistors, Nano Lett. 6 (2006) 1454–1458.
[5] R. Könenkamp, R.C. Word, M. Godinez, Ultraviolet electroluminescence from ZnO/polymer heterojunction light-emitting diodes, Nano Lett. 5 (2005) 2005–2008.
[6] J.M. Bao, M.A. Zimmler, F. Capasso, X.W. Wang, Z.F. Ren, Broadband ZnO single-nanowire light-emitting diode, Nano Lett. 6 (2006) 1719–1722.
[7] E. Galoppini, J. Rochford, H.H. Chen, G. Saraf, Y.C. Lu, A. Hagfeldt, G. Boschloo, Fast electron transport in metal organic vapor deposition grown dye-sensitized ZnO nanorod solar cells, J. Phys. Chem. B 110 (2006) 16159–16161.
[8] T.P. Chou, Q. Zhang, G.E. Fryxell, G.Z. Cao, Hierarchically structured ZnO film for dye-sensitized solar cells with enhanced energy conversion efficiency, Adv. Mater. 19 (2007) 2588–2592.

[9] A. Umar, Y.B. Hahn, Large-quantity synthesis of ZnO hollow objects by thermal evaporation: growth mechanism, structural and optical properties, Appl. Surf. Sci. 254 (2008) 3339–3346.
[10] Y.C. Kong, D.P. Yu, B. Zhang, W. Fang, S.Q. Feng, Ultraviolet-emitting ZnO nanowires synthesized by a physical vapor deposition approach, Appl. Phys. Lett 78 (2001) 407–409.
[11] X.Y. Kong, Y. Ding, R. Yang, Z.L. Wang, Single-crystal nanorings formed by epitaxial self-coiling of polar-nanobelts, Science 303 (2004) 1348–1351.
[12] J.L. Campbell, M. Breedon, K. Latham, K.K. Zadeh, Electrowetting of superhydrophobic ZnO nanorods, Langmuir 24 (2008) 5091–5098.
[13] C. Ronning, P.X. Gao, Y. Ding, Z.L. Wang, D. Schwen, Manganese doped ZnO nanobelts for spintronics, Appl. Phys. Lett. 84 (2004) 783–785.
[14] R.C. Wang, C.P. Liu, J.L. Huang, S.J. Chen, ZnO symmetric nanosheets integrated with nanowalls, Appl. Phys. Lett. 87 (2005) 053103.
[15] A. Umar, Y.B. Hahn, ZnO nanosheet networks and hexagonal nanodiscs grown on silicon substrate: growth mechanism and structural and optical properties, Nanotechnology 17 (2006) 2174–2180.
[16] H.B. Zeng, W.P. Cai, P.S. Liu, X.X. Xu, H.J. Zhou, C. Klingshirn, H. Kalt, ZnO-based hollow nanoparticles by selective etching: elimination and reconstruction of metal-semiconductor interface, improvement of blue emission and photocatalysis, ACS Nano 2 (2008) 1661–1670.
[17] H.Q. Wang, G.H. Li, L.C. Jia, G.Z. Wang, C.J. Tang, Controllable preferential-etching synthesis and photocatalytic activity of porous ZnO nanotubes, J. Phys. Chem. C 112 (2008) 11738–11743.
[18] X.M. Sun, J.F. Liu, Y.D. Li, Use of carbonaceous polysaccharide microspheres as templates for fabricating metal oxide hollow spheres, Chem. Eur. J. 12 (2006) 2039–2047.
[19] F. Caruso, Hollow capsule processing through colloidal templating and self-assembly, Chem. Eur. J. 6 (2000) 413–419.
[20] J.Q. Hu, Q. Li, X.M. Meng, C.S. Lee, S.T. Lee, Thermal reduction route to the fabrication of coaxial Zn/ZnO nanocables and ZnO nanotubes, Chem. Mater. 15 (2003) 305–308.
[21] P.A.R. Tafulo, M. Ferro, A. Guerreiro, G.G. Aguilar, Engineering the crystal growth behavior: "On substrate" MOD formation of ZnO hollow spheres, Appl. Surf. Sci. 256 (2010) 3281–3285.
[22] Z.W. Deng, M. Chen, G.X. Gu, L.M. Wu, A facile method to fabricate ZnO hollow spheres and their photocatalytic property, J. Phys. Chem. B 112 (2008) 16–22.
[23] K.M. Sulieman, X.T. Huang, J.P. Liu, M. Tang, Controllable synthesis and characterization of hollow-opened ZnO/Zn and solid Zn/ZnO single crystal microspheres, Nanotechnology 17 (2006) 4950–4955.
[24] J. Liu, X.L. Chen, W.J. Wang, Q.S. Huang, G. Wang, K.X. Zhu, J.G. Guo, Large scale synthesis of porous ZnO hollow structures with tunable diameters and shell thicknesses, Mater. Lett. 63 (2009) 2221–2223.
[25] R.S. Wagner, W.C. Ellis, Vapor liquid solid mechanism of single crystal growth, Appl. Phys. Lett. 4 (1964) 89–90.
[26] M.H. Huang, Y.Y. Wu, H. Feick, N. Tran, E. Weber, P.D. Yang, Catalytic growth of zinc oxide nanowires by vapor transport, Adv. Mater. 13 (2001) 113–116.
[27] D. Banerjee, J.Y. Lao, D.Z. Wang, J.Y. Huang, D. Steeves, B. Kimball, Z.F. Ren, Synthesis and photoluminescence studies on ZnO nanowires, Nanotechnology 15 (2004) 404–409.
[28] W.Y. Chen, R.C. Wang, C.P. Liu, Substrate effect induced growth of various single-crystalline Zn and Zn/ZnO core–shell polyhedrons with tunable photoemission, Cryst. Growth Des. 8 (2008) 2248–2255.
[29] Y.H. Yang, B. Wang, G.W. Yang, Mechanisms of self-catalyst growth of agave-like zinc oxide nanostructures on amorphous carbons, Cryst. Growth Des. 7 (2007) 1242–1245.
[30] Y.H. Yang, B. Wang, G.W. Yang, Growth mechanisms of one-dimensional zinc oxide hierarchical structures, Nanotechnology 17 (2006) 5556–5560.
[31] C.C. Lin, K.H. Liu, S.Y. Chen, Growth and characterization of Zn–ZnO core–shell polygon prismatic nanocrystals on Si, J. Cryst. Growth 269 (2004) 425–431.
[32] K.H. Liu, C.C. Lin, S.Y. Chen, Growth and physical characterization of polygon prismatic hollow Zn–ZnO crystals, Cryst. Growth Des. 5 (2005) 483–487.
[33] H.J. Fan, R. Scholz, F.M. Kolb, M. Zacharias, U. Gösele, Growth mechanism and characterization of ZnO microcages, Solid State Commun. 130 (2004) 517–521.
[34] A. Sekar, S.H. Kim, A. Umar, Y.B. Hahn, Catalyst-free synthesis of ZnO nanowires on Si by oxidation of Zn powders, J. Cryst. Growth 277 (2005) 471–478.
[35] L.F. Xu, Y. Guo, Q. Liao, J.P. Zhang, L.S. Xu, Morphological control of ZnO nanostructures by electrodeposition, J. Phys. Chem. B 109 (2005) 13519–13522.